Effects of Oscillatory Electric Fields on Internal Membranes: An Analytical Model

Vijayanand Vajrala,* James R. Claycomb,*† Hugo Sanabria,*‡ and John H. Miller Jr.*
*Department of Physics and Texas Center for Superconductivity, University of Houston, Houston, Texas; †Department of Mathematics and Physics, Houston Baptist University, Houston, Texas; and ‡University of Texas Health Science Center, Houston, Texas

ABSTRACT We derive an analytical model of the potential differences induced across plasma and internal organelle membranes in suspended cells exposed to oscillatory electric fields. Multiple shells are modeled using iterative applications of the single-shell calculation with mobile charges. This work is motivated, in part, by recent results suggesting the ability to use alternating current (ac) fields to noninvasively monitor enzyme activity within internal membranes, particularly the mitochondrial electron transport chain. Previous work, on induced transmembrane voltages in cells subjected to ac fields, has mainly been limited to oscillatory potentials across the plasma membrane. Here we first develop a three-membrane model, consisting of a plasma membrane surrounding inner and outer membranes representing an internal organelle, such as a mitochondrion. Frequency-dependent transmembrane potentials are modeled for spherical, weakly conducting membrane shells enclosing a conductive cytoplasm surrounding an idealized internal organelle. We then use a two-shell model to simulate induced ac membrane potentials of a suspended isolated mitochondrion in which the outer membrane is usually much more permeable than the inner membrane.

INTRODUCTION

Time-varying electric fields can induce a number of biophysical responses when applied to live cells. One phenomenon of interest is electroporation, also known as electropermeabilization, in which a rapidly time-varying field increases the permeability of the plasma membrane. This enables the introduction into cells of molecules to which the plasma membrane would otherwise be impermeable. Electroporation is increasingly being used for the treatment of solid cutaneous and subcutaneous tumors (1) and holds promise for gene therapy (2).

Oscillatory electric fields can also modulate the conformational states of membrane proteins. This has been demonstrated extensively for pumps in the outer plasma membrane (3–7). Membrane proteins are candidates for nonlinear behavior since they cannot rotate within the membrane and dissipate energy through Debye-like relaxation, and since any transmembrane domains with dipole moments interact with the external alternating current (ac) field. The oscillatory transmembrane potential adds to any existing potential to modulate the conformational states of membrane proteins and can even induce pumps to transport ions (3,4). The combination of protein conformational changes and ion translocation creates a nonlinear response manifested by the generation of harmonics (5). Cyclic processes, such as ion transport, ATP consumption, and respiratory processes (6), are of particular interest because they are sensitive to synchronization by an oscillatory field. Model calculations by Tsong (7) demonstrate that interactions of protein dipole moments with electrically modulated membrane potentials induce conformational changes that can result in harmonic generation. Measurement of linear impedance or nonlinear harmonic response, of live cell suspensions or live tissue, is potentially useful as an assay to monitor the collective behavior of large numbers of cells in real time.

Of perhaps greater importance is the possibility of using ac electric fields to noninvasively monitor internal processes, in mitochondria or other organelles, that cannot readily be probed using established techniques such as voltage- and patch-clamp methods. By sweeping the applied fundamental frequency, one can obtain detailed harmonic spectra that reveal information about the timescales of enzyme activity. For example, recent experiments (8) show that second and higher harmonics generated by whole organisms, mitochondria, and chloroplasts, in response to sinusoidal fields of several volts per centimeter amplitude, correlate with activation or inhibition of complexes in the mitochondrial electron transport chain (ETC). At low frequencies, below a few hundred hertz, the induced harmonics are primarily produced by pumps in the outer plasma membrane (9,10). However, as the applied frequency is increased into the kilohertz range, the ac field capacitively couples through the plasma membrane, allowing this method to probe internal organelles.

The enzyme complexes responsible for ATP production in the mitochondrial inner membranes, including the remarkable molecular turbine ATP synthase as well as those responsible for photosynthesis in plant cells in the thylakoid membranes of chloroplasts, produce features in harmonic generation spectra at kilohertz frequencies (8). These complexes are of fundamental interest since the bioenergetic mechanisms by which they engage in either oxidative metabolism or photosynthesis are of extremely ancient origin

Submitted June 7, 2007, and accepted for publication November 12, 2007.

Address reprint requests to James. R. Claycomb, E-mail: jclaycomb@hbu.edu.

Editor: Meyer B. Jackson.

0006-3495/08/03/2043/10 $2.00

doi: 10.1529/biophysj.107.114611

and are essential to life on Earth. The ability to detect respiratory activity in the mitochondrial inner membrane, either in vivo or ex vivo, could also lead to important medical applications, since mitochondrial dysfunction has been linked to type II diabetes (11), heart disease (12), cancer (13,14), Alzheimer's disease (15), and numerous specific mitochondrial disorders. The motivation for this work is thus to determine the extent to which an ac field can induce an oscillatory potential across an internal membrane, which would add to any intrinsic membrane potential and could potentially affect both the linear and nonlinear ac responses of mitochondrial ETC and other internal membrane complexes.

The outer cell membrane is a partially permeable boundary surrounding the cytoplasm and intracellular organelles and is made up of lipids and proteins. This outer lipid membrane, an electrical insulator by nature, experiences most of the potential drop across its boundary when the cell is subjected to applied electric fields at very low frequencies. Modulation of the plasma membrane potential leads to conformational changes in proteins and enzymes embedded within the membrane. The induced potential drop, caused by low membrane permittivity and conductivity, as well as the rearrangement of interfacial charges, gives rise to field changes on the order of 0.75 kV/cm across the 5-nm thickness of the membrane, for a 1.0 V/cm field strength. At frequencies below $\sim 10^4$ Hz, the interior of the cell is screened from the applied electric field. At higher frequencies, the electric field is coupled capacitively through the membrane, whereas the counterions are not sufficiently mobile to screen the interior of the cell so that potential drops are induced across intracellular organelle membranes. Mitochondria, which incorporate a dual membrane structure, play a key role in the energy metabolism of cells. It has been shown that the induced transmembrane potential developed in mitochondrial membranes may affect cellular metabolisms.

The earliest analytical description of electric field-induced voltages across outer cell membranes dates back to 1950 (16). In this pioneering work, Schwan derived an expression for the induced steady-state transmembrane voltage drop for a spherical cell given by, in the low-frequency limit,

$$\Delta\Phi = \frac{3}{2} E_0 R \cos\theta, \tag{1}$$

where E_0 is the external electric field, R is the cell radius, and θ is the polar angle measured from the center of the cell with respect to the direction of the field. At finite frequencies, the induced ac transmembrane potential for a spherical cell becomes (17)

$$\Delta\Phi(\omega) = \frac{3}{2} \cos\theta \frac{E_0 R}{1 + j\omega\tau}, \tag{2}$$

where τ is the charging time constant of the membrane and $\omega = 2\pi f$.

Kotnik (18) developed a steady-state formula for induced transmembrane potential that embodies the conductivities of intracellular, membrane, and extracellular regions of the cell. Fricke measured the transmembrane voltage of an ellipsoidal cell with negligible membrane conductance surrounded by a highly conductive cytoplasm (19). Based on these measurements, he developed an empirical expression for the induced transmembrane potential difference $\Delta\Phi_a = aE_0/(1 - n_a)$ where a denotes the semimajor axis oriented in the field direction and n_a is the depolarizing factor along a.

Bryant and Wolfe (20) obtained an analytical solution for the transmembrane potential difference across prolate spheroidal nonconducting cell membranes. Later, Jerry (21) derived an expression for the transmembrane potential difference across spheroidal conducting cell membranes. Gimsa and Wachner (22) solved for the field-induced forces and transmembrane voltages on spheroidal cells and, more recently, for the induced transmembrane voltage drops for arbitrarily oriented ellipsoidal and cylindrical cells (23). The induced membrane potential across arbitrarily shaped cellular membranes with mobile surface charges was calculated by Prodan and Prodan in describing the dielectric behavior of living cell suspensions (24).

Asami and Irimajiri (25) employed a double-shell model to extract electrical parameter values from dielectric response measurements of intact mitochondria. More recently, Kotnik and Miklavčič calculated the ac transmembrane voltage induced on spheroidal cells (26) and across internal membranes, using a double-shell model for application to cells exposed to nanosecond-duration pulsed electric fields (27). Their model showed that induced organelle membrane potentials can exceed the potential drop across the plasma membrane at certain frequencies and electrical parameter values. When cells are subjected to low-frequency electric fields (below $\sim 10^2$ Hz), almost the entire external macroscopic field is attenuated across the plasma membrane. The redistribution of counterions outside of the cell results in a substantial amplification of the resting potential across the plasma membrane. Counterions effectively serve as a high-pass filter shielding the organelles from low-frequency external fields. Induced transmembrane potentials may activate enzymes in the plasma membrane, resulting in a nonlinear response to the excitation field manifest as harmonics of the excitation frequency.

Nonlinear harmonic response measurements of yeast cells have been made with both single (5) and double (28) frequency excitations and by using a SQUID magnetometer (9,29). The generation of harmonics was inhibited by low concentrations of sodium metavanadate, suggesting that the nonlinearity is largely attributed to H^+-ATPase present in the plasma membranes of the cells. At higher frequencies (above $\sim 10^3$ Hz), the plasma membrane can no longer screen the interior of the cell and membrane potentials are modulated across organelle membranes. Around 10^4 Hz, electrically excitable internal organelles may generate harmonics due to processes within ETC complexes governing ATP synthesis in mitochondria and chloroplasts (8).

In this work we develop two- and three-shell models to solve for the induced potentials across mitochondrial membranes in isolated mitochondria and mitochondria in whole cells, respectively. An approximation is used where nested shells are modeled using repeated applications of the single-shell calculation. This simplifies the analysis by using the fact that the ac electric field inside a single dielectric conducting spherical shell is uniform. The main objective of this work is to calculate the induced transmembrane potentials across the plasma and mitochondrial membranes. Our analysis takes into account mobile surface charges on the plasma and mitochondrial membranes. Frequency-dependent transmembrane potentials are calculated across each membrane for several electrical parameter values obtained from the literature (18,30,31).

MATERIALS AND METHODS

We calculate the induced transmembrane potential differences in nested spherical shelled cells with interfacial distributions of free charges on the faces of the membranes. In a realistic cellular environment, the free charges are distributed spatially rather than on the surface. The free charge distribution is treated as surface because the charge distribution is practically zero for distances larger than 10^{-9} m from the membrane. Thus this approach serves particularly well for the induced transmembrane potentials across the mitochondrial membranes.

We consider a three-membrane model of the cell containing mitochondria and a two-membrane isolated mitochondrion model. The outer shell of the three-membrane model represents the plasma membrane. The middle and innermost membranes represent mitochondrial outer and inner membranes. A surface charge distribution is specified on the outer faces of each shell. Numerical values of the conductivity, permittivity, and mobility of various cellular tissue regions are obtained from Kotnik et al. (18) and Schoenbach (30) with surface charge densities from Yang et al. (31). The ac-induced transmembrane potential is superimposed on the resting transmembrane potential, thereby modulating the membrane potential. These changes in the membrane potential induce dipole moments, enabling interaction with other cells in a suspending cell medium by changing the charge distributions surrounding intracellular organelles. As a result, the external field is modified.

The intensity of the above effects will vary between mitochondria, which are close to the nuclear envelope and those closer to the center of the cell. The resulting spatial charge distribution is complex and needs to be modeled in three dimensions. The mutual interactions between induced dipoles lead to a many-body problem without an exact analytical solution for the induced potentials across the membranes. Hence in this work, to minimize the complexity involved in the many-body system, we ignore dipole interactions between cells in suspension and between neighboring mitochondria and other organelles within the cell. To meet the above requirement, we assume a dilute cell suspension with fractional volume concentration of the spherical particles <0.05 minimal interactions between the particles in the suspension. In an actual cell, there are a large number of mitochondria; however, we consider a single mitochondrion at the center of the cell in our model. This simplified treatment is facilitated by a mitochondrial volume fraction ≈ 0.01 within the cell and the nearly uniform excitation field that penetrates the cell.

If a single-shelled dielectric particle with surface charge distribution is exposed to an ac applied field, then the potential Φ_m obeys Poisson's equation

$$\nabla^2\Phi_m = -\frac{1}{\varepsilon_m}\sum_i \rho_{m,i}, \tag{3}$$

where $\rho_{m,i}$ and ε_m are the charge density and permittivity in the cytoplasm, cell membrane, and extracellular space corresponding to $m = 1$, 2, and 3, respectively. The current density J_m in each dielectric medium is given by

$$J_m = -\sum_i(\sigma_{m,i}\nabla\Phi_m - D_{m,i}\nabla\rho_{m,i}), \tag{4}$$

where $\sigma_{m,i}$ is the conductivity, $\rho_{m,i}$ is the volume charge density, and $D_{m,i}$ is the diffusion coefficient. $D_{m,i}$ is proportional to the charge mobility $\mu_{m,i}$ according to Einstein's equation

$$D_{m,i} = \frac{\mu_{m,i}}{q_i}kT, \tag{5}$$

where k is the Boltzmann constant and T is the absolute temperature. The charge is given by $q_i = Z_i e$, where e is the electronic charge and Z_i is the valence of the ith species. In general, the conductivity $\sigma_{m,i}$ will depend on the charge density (32)

$$\sigma_{m,i} = \frac{D_{m,i}q_i\rho_{m,i}}{kT}. \tag{6}$$

Including this dependence on charge density, the divergence of J_m gives

$$\nabla\cdot J_m = -\sum_i\left(\frac{D_{m,i}q_i}{kT}\nabla\cdot(\rho_{m,i}\nabla\Phi_m) - D_{m,i}\nabla^2\rho_{m,i}\right). \tag{7}$$

Using the identity $\nabla\cdot(\rho\nabla\Phi) = \nabla\Phi\cdot\nabla\rho + \rho\nabla^2\Phi$, the continuity equation

$$\nabla\cdot J_m = -j\omega\sum_i\rho_{m,i} \tag{8}$$

and Poisson's equation, Eq. 6 become

$$\sum_i\frac{D_{m,i}q_i}{kT}\left(\nabla\Phi\cdot\nabla\rho_{m,i} - \frac{\rho_{m,i}^2}{\varepsilon_m}\right) + \sum_i D_{m,i}\nabla^2\rho_{m,i} = j\omega\sum_i\rho_{m,i}, \tag{9}$$

where $j = \sqrt{-1}$. The general solution for the potential and charge distribution is nonlinear, requiring the simultaneous numerical solution of Eqs. 9 and 3. In the following analysis we develop an analytical approximation for the charge density perturbation on each membrane surface and then solve for the resulting induced potentials using Eq. 3. We first consider the high-frequency limit where the conduction current is much greater than the diffusion current $\sigma\nabla\Phi \gg D\nabla\rho$ so we can neglect the $\nabla^2\rho$ term, thus

$$\nabla\Phi\cdot\nabla\rho - \frac{\rho^2}{\varepsilon} = \frac{j\omega kT}{Dq}\rho \tag{10}$$

after removing the summations and suppressing subscripts for simplicity. We then approximate $-\nabla\Phi$ with the value of the external field E_0 on the outer membrane and by the screened electric field $a(\omega)$ on internal membranes. At the polar cap, where $\nabla\rho$ is maximal, $\nabla\rho = \hat{r}\partial\rho/\partial r$ so $\nabla\Phi\cdot\nabla\rho \approx -E_0\partial\rho/\partial r$ and we have the first-order differential equation for the charge perturbation

$$\varepsilon E_0\frac{\partial\rho}{\partial r} + \rho^2 + \frac{j\omega\varepsilon kT}{Dq}\rho = 0. \tag{11}$$

The differential equation

$$\alpha\frac{\partial\rho}{\partial r} + \rho^2 + \beta\rho = 0, \tag{12}$$

where $\alpha = \varepsilon E_0$ and $\beta = j\omega\varepsilon kT/Dq$, has solution

$$\rho = \frac{\beta}{\exp\left(\frac{\beta r}{\alpha} - \beta C_1\right) - 1}. \tag{13}$$

We construct the integration constant C_1 so $\rho(\omega \to \infty) = 0$ and so ρ falls off from the surface of the membrane R. If we take

$$C_1 = \frac{1}{\beta}\left[\ln\left(\frac{\alpha}{\beta\delta}\right)^2 + \frac{\beta^2}{\alpha}R\right] \tag{14}$$

the charge perturbation becomes

$$\rho = \frac{\beta}{\left(\frac{\beta\delta}{\alpha}\right)^2 \exp\left(\frac{\beta}{\alpha}(r-R)\right) - 1}. \tag{15}$$

Further replacing $r - R$ by the effective thickness of the charge density layer taken to be the Debye screening length $\delta = 0.7$ nm for Ringer's solution and multiplying by δ to obtain the surface charge density $\lambda = \rho\delta$ in C/m^2 we have

$$\lambda(\omega) = \frac{\frac{\omega\varepsilon kT\delta}{jDq}}{1 + \left(\frac{\omega kT\delta}{DqE_0}\right)^2 \exp\left(j\frac{\omega kT\delta}{DqE_0}\right)}. \tag{16}$$

This expression is zero at direct current (dc), and the argument of the exponential is pure imaginary with magnitude $10^{-10} - 10^{-4}$ between $1 - 10^6$ Hz for an external field of 1.0 V/cm. In our model we choose the maximum charge perturbation based on the measured surface charge density at dc $\lambda(\omega \to 0) = \lambda_{n,0}$, with values between $10^{-3} \sim 10^{-2} C/m^2$ (31) on the inner and outer surfaces of the membrane. Writing the $\cos(\theta)$ dependence explicitly, we have the charge perturbation

$$\lambda_n(\omega) = \frac{\lambda_{n,0}}{1 + \frac{j\omega kT\delta}{D_m qE_0}}\cos(\theta) \tag{17}$$

on the nth membrane surface. For internal membranes,E_0 is replaced by the screened electric field $a(\omega)$. This equation is similar in form to Eq. 2 for the induced membrane potential with inverse frequency dependence at high frequencies. The diffusion constants D_m are given by their values just outside the membrane surfaces. When the particle in suspension is excited by an external ac electric field, the interior and exterior potentials obey Laplace's equation with boundary conditions on each surface. The solution for the scalar potential Φ_m in each region is given by

$$\Phi_1 = \sum_{l=0}^{\infty} a_l r^l P_l(\cos\theta) \tag{18}$$

$$\Phi_2 = \sum_{l=0}^{\infty} b_l r^l + c_l r^{-(l+1)} P_l(\cos\theta) \tag{19}$$

$$\Phi_3 = -E_0 r\cos\theta + \sum_{l=0}^{\infty} d_l r^{-(l+1)} P_l(\cos\theta), \tag{20}$$

where again m=1, 2, and 3 corresponds to interior, membrane, and exterior regions, respectively. The coefficients a_l,b_l,c_l, and d_l are determined from the continuity of the potential and discontinuity in normal displacement,

$$\Phi_m(r_n) = \Phi_{m+1}(r_n) \tag{21}$$

$$\varepsilon^*_{m+1}\frac{\partial\Phi_{m+1}}{\partial r}\bigg|_{r_n} - \varepsilon^*_m\frac{\partial\Phi_m}{\partial r}\bigg|_{r_n} = \lambda_n, \tag{22}$$

on the nth surface ($n = 1, 2$). The complex permittivity ε^*_m and conductivity σ^*_m are given by

$$\varepsilon^*_m = \varepsilon_m + \frac{\sigma_m}{j\omega\varepsilon_0} \tag{23}$$

$$\sigma^*_m = \sigma_m + j\omega\varepsilon_0\varepsilon_m, \tag{24}$$

with relative permittivity ε_m and conductivity σ_m, respectively. The conductivities σ_m should be given as the sum over each species $\Sigma a_i\sigma_{m,i}$ with fractional weights a_i. In our model we use the measured conductivity values tabulated in Table 1.

RESULTS AND DISCUSSION

Three-membrane model

We first model a single cell of diameter 100 μm containing a single mitochondrion with a 0.5-μm radius at the center. Three shells representing the outer plasma membrane and outer mitochondrial membrane (OMMs) and inner mitochondrial membranes (IMMs) partition the cell with the dimensions shown in Fig. 1. Parameter values, including permeabilities and diffusion coefficients, are also given in Table 1. The potential distribution enclosed by, within, and surrounding a single-membrane particle in suspension with alternating excitation field amplitude E_0 may be written in Cartesian coordinates

$$\Phi_1 = a(\omega)x \tag{25}$$

$$\Phi_2 = b(\omega)x + \frac{c(\omega)x}{(x^2 + y^2)^{3/2}} \tag{26}$$

$$\Phi_3 = -E_0 x + \frac{d(\omega)x}{(x^2 + y^2)^{3/2}}, \tag{27}$$

TABLE 1 Electrical parameter and geometrical factors used in the two-membrane mitochondria and three-membrane cell models

Parameter	Value
Extra cellular conductivity	2.0 S/m
Membrane conductivity	5.0×10^{-8} S/m
Intracellular conductivity	0.95 S/m
Extracellular permittivity	80.0 ε_0
Membrane permittivity	16.8 ε_0
Intracellular permittivity	87.7 ε_0
Diffusion constant outside the cell membrane	2.07×10^{-10} m^{2}s^{-1}
Diffusion constant inside the cell membrane	2.07×10^{-9} m^{2}s^{-1}
OMM conductivity	0.95×10^{-6} S/m
OMM permittivity	12.1 ε_0
Mitochondrial intramembranous conductivity	0.4 S/m
Mitochondrial intramembranous permittivity	54.0 ε_0
Diffusion constant on outside OMM	2.07×10^{-9} m^{2}s^{-1}
Diffusion constant on inside OMM	9.3×10^{-9} m^{2}s^{-1}
IMM conductivity	0.95×10^{-6} S/m
IMM permittivity	5.0 ε_0
Mitochondrial matrix conductivity	0.001–0.1 S/m
Mitochondrial matrix permittivity	54.0 ε_0
Diffusion constant on outside IMM	9.3×10^{-9} m^{2}s^{-1}
Diffusion constant on inside IMM	1.0×10^{-9} m^{2}s^{-1}
Outer radius of the plasma membrane	5.0×10^{-5} m
Inner radius of the plasma membrane	4.999×10^{-5} m
Outer radius of the OMM	50.0×10^{-8} m
Inner radius of the OMM	49.3×10^{-8} m
Outer radius of the IMM	48.5×10^{-8} m
Inner radius of the IMM	47.8×10^{-8} m

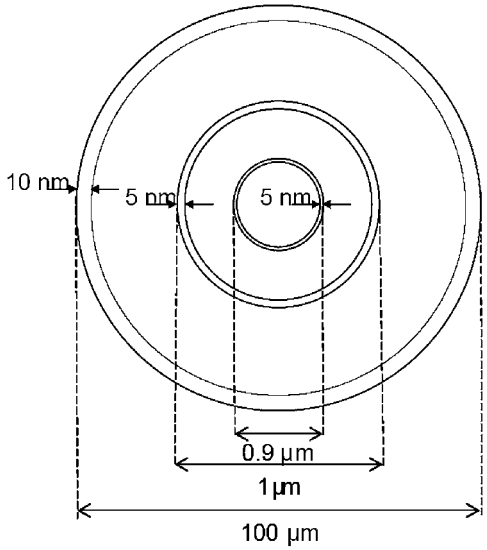

FIGURE 1 Schematic of the three-membrane cell model. The outer shell represents the plasma membrane, and the inner two shells represent the OMMs and IMMs.

where $a(\omega), b(\omega), c(\omega)$, and $d(\omega)$ are obtained from the boundary conditions (14) and (15), or

$$a(\omega) = \frac{2a^3\lambda_1(\varepsilon_2^* - \varepsilon_3^*) + b^3(\lambda_1(2\varepsilon_3^* + \varepsilon_2^*) + 3\varepsilon_2^*(\lambda_2 - 3E_0\varepsilon_3^*))}{r(\omega)} \tag{28}$$

$$b(\omega) = \frac{2a^3\lambda_1(\varepsilon_2^* - \varepsilon_3^*) + b^3(6E_0\varepsilon_3^*(\varepsilon_1^* - \varepsilon_2^*) + 2\lambda_2(\varepsilon_1^* + \varepsilon_2^*))}{r(\omega)} \tag{29}$$

$$c(\omega) = \frac{a^3b^3((3\varepsilon_3^*E_0 + \lambda_2)(\varepsilon_1^* - \varepsilon_2^*) + \lambda_1(2\varepsilon_3^* + \varepsilon_2^*))}{r(\omega)} \tag{30}$$

$$d(\omega) = \frac{b^6(E_0(2\varepsilon_2^* + \varepsilon_1^*)(\varepsilon_2^* - \varepsilon_3^*) + 2\lambda_2(\varepsilon_2^* - \varepsilon_1^*))}{r(\omega)} + \frac{a^3b^3((E_0(2\varepsilon_2^* + \varepsilon_3^*) - \lambda_2)(\varepsilon_1^* - \varepsilon_2^*) + 3\varepsilon_2^*\lambda_1)}{r(\omega)} \tag{31}$$

where

$$r(\omega) = 2a^3(\varepsilon_1^* - \varepsilon_2^*)(\varepsilon_2^* - \varepsilon_3^*) + b^3(\varepsilon_1^* + 2\varepsilon_2^*)(\varepsilon_2^* + 2\varepsilon_3^*). \tag{32}$$

The electric field enclosed by the plasma membrane is the gradient of the potential Φ_1 or $\mathbf{E} = a(\omega)\hat{\mathbf{i}}$, so that the field inside the single shell is uniform. The potential distribution near a second membrane with a radius much smaller than the outer membrane is thus obtained by substituting $a(\omega)$ for E_0 in the expressions above. The potential near the mitochondrial inner (third) membrane may be calculated in a similar manner. The potential difference across each membrane may then be determined as a function of frequency.

Fig. 2, *a* and *b*, shows the uniform electric field inside and potential distribution near the outer 10-nm thick membrane

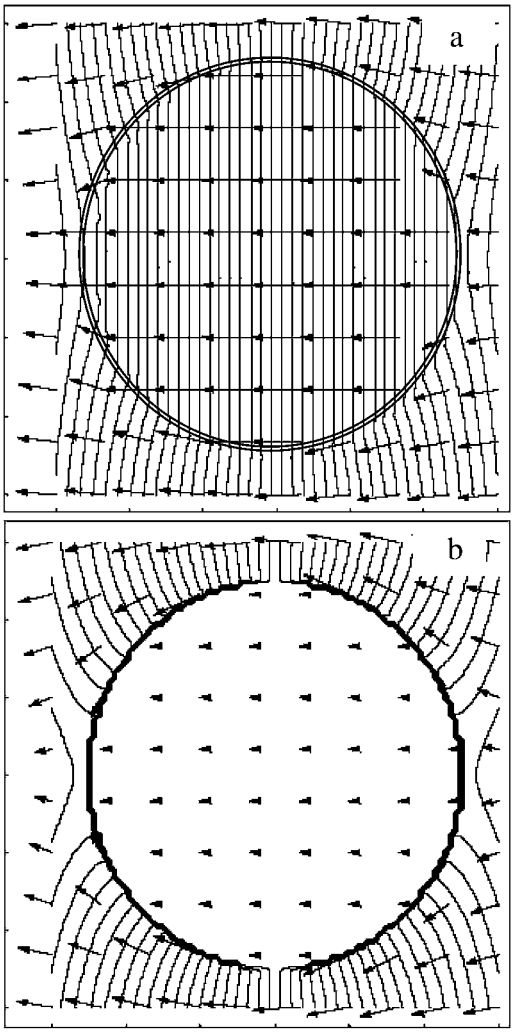

FIGURE 2 Electric field vector plot and potential distribution near the plasma membrane with mobile surface charges in an alternating electric field. The uniform electric field in the cell is greater at (*a*) 10^6 Hz than at (*b*) 10^2 Hz. The excitation field is 1.0 V/cm.

without external charges at 100 kHz and 100 Hz, respectively. Fig. 3 shows the frequency-dependent induced plasma membrane potential (*a*) without and (*b*) with a surface charge density of 0.01 C/m^2 on the outer membrane surface for a 1 V/cm excitation. The induced potential without surface charges is 7.5 mV up to 10^4 Hz, decreasing mostly between 10^5 and 10^6 Hz. The induced plasma membrane potential with surface charges increases an additional 0.25 mV between $\sim 10^2$ and 10^5 Hz compared to those without surface charges.

Induced OMM potentials are shown in Fig. 4 *a* without and *b* with surface charges in a 1 V/cm ac field excitation. The maximum induced potential of 60 μV occurs near 1 MHz both with and without surface charges. The induced OMM potential with surface charges increases an additional 5 μV between $\sim 10^2$ and 10^4 Hz.

IMM induced potentials are shown in Fig. 5 *a* without and *b* with surface charges in a 1 V/cm ac field excitation. The

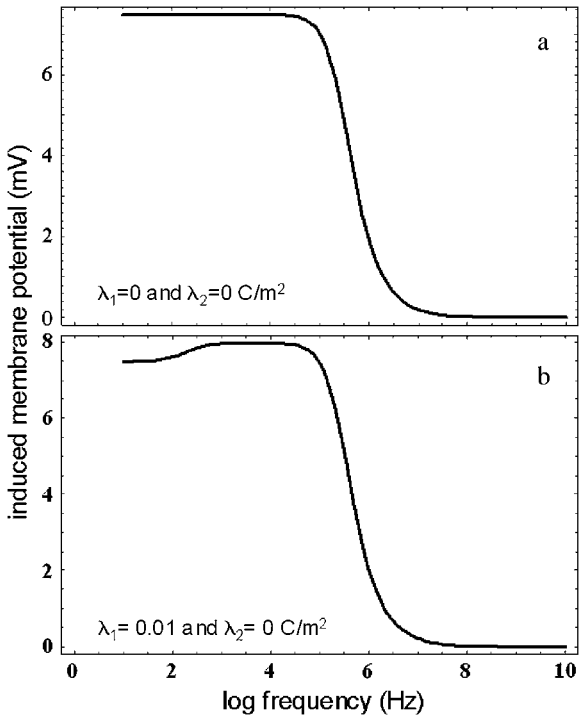

FIGURE 3 Variation of the induced potential across the plasma membrane with frequency of the excitation field in the whole cell, three-membrane model (*a*) without free charges and (*b*) with a surface charge density of 0.01 C/m^2 on the outer and 0.001 C/m^2 on the inner membrane surface. The excitation field is 1.0 V/cm.

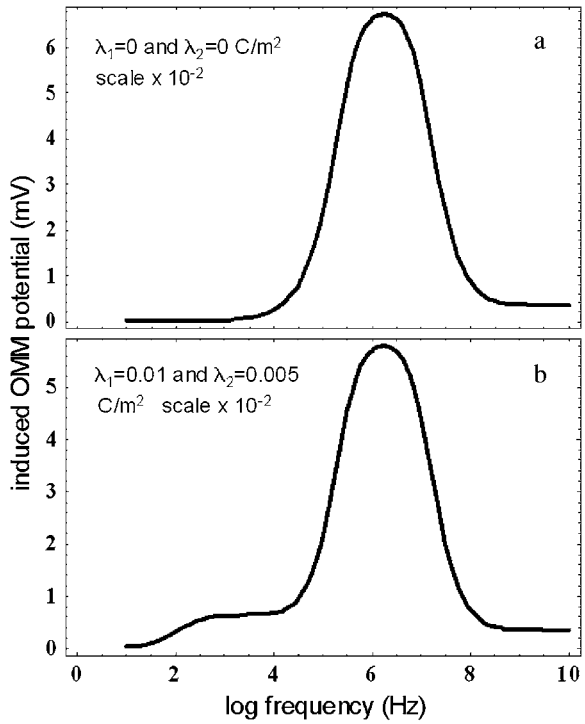

FIGURE 4 Variation of the induced potential across the OMM with frequency of the excitation field in the whole cell, three-membrane model (*a*) without free charges and (*b*) with a surface charge density of 0.01 C/m^2 on the outer and 0.001 C/m^2 on the inner membrane surface. The excitation field is 1.0 V/cm.

maximum induced potential occurs slightly higher than 1 MHz both with and without surface charges. The induced IMM potential begins to increase near 1 kHz with surface charges compared to 100 kHz without surface charges. The maximum induced IMM potential is nearly three times greater with the surface charge densities in Fig. 5 *b* compared to the absence of charges in *a*.

Two-membrane model

We developed a two-membrane model to simulate ac-induced membrane potentials in isolated mitochondria in suspension. In this model, the two inner membranes shown in Fig. 1 correspond to OMMs and IMMs, with electrical parameter values given in Table 1. A 1-μm diameter mitochondrion is exposed to the same time harmonic electric field as before. The induced potentials on the outer membrane are obtained from Eqs. 18–20 with boundary conditions as in Eqs. 21 and 22.

Induced OMM potentials are shown in Fig. 6 *a* without and *b* with surface charges in a 1 V/cm field excitation. The induced potential is 74 μV without and ~78 μV with surface charges up to 1 MHz with both potential curves decreasing mostly between 1 and 100 MHz. This induced OMM potential differs from that of the three-membrane model where the plasma membrane screens the interior of the cell so that no potential drop is observed across the mitochondrial membranes at lower frequencies.

Induced potentials on the IMM in the two-membrane model are shown in Fig. 7 *a* without and *b* with surface charges for a 1 V/cm excitation. The maximum induced potential occurs near 10 MHz both with and without mobile charges. The maximum induced potential with surface charges is an order of magnitude greater than the potential without mobile surface charges. The induced IMM potential with mobile surface charges increases ~0.1 mV between 100 Hz and 1 MHz, as can be seen in the plateau just before the peak in Fig. 7 *b*. Fig. 8 shows the change in IMM potential for matrix conductivities of (*a*) 0.1, (*b*) 0.01, and (*c*) 0.001 S/m. In this figure, the maximum potential increases from 0.76 to 17.5 mV, whereas the peak frequency decreases from 10 MHz to 10 kHz, as the matrix conductivity is decreased from 0.1 to 0.001 S/m.

CONCLUSIONS

In this work, we have modeled membrane potentials induced by alternating electric fields on nested spherical membranes in suspension with and without mobile charges near the membranes. Our model employs an iterative procedure to calculate the induced potential across each membrane, using

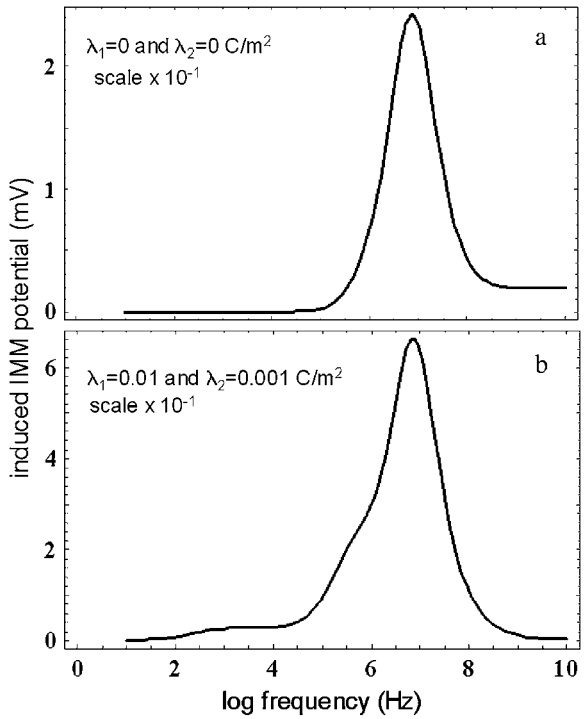

FIGURE 5 Variation of the induced potential across the IMM with frequency of the excitation field in the whole cell, three-membrane model (*a*) without free charges and (*b*) with a surface charge density of 0.01 C/m^2 on the OMM and 0.001 C/m^2 on the IMM surface. The excitation field is 1.0 V/cm.

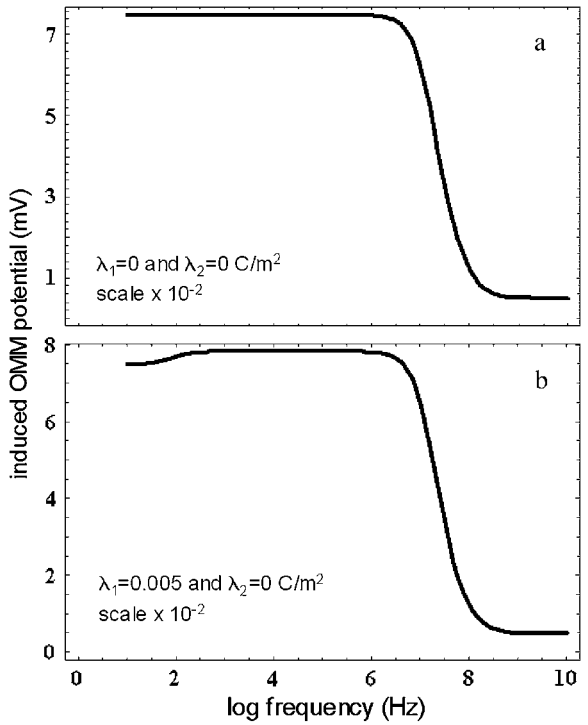

FIGURE 6 Variation of the induced potential across the OMM with frequency of the excitation field in the isolated mitochondrion, two-membrane model (*a*) without free charges and (*b*) with a surface charge density of 0.01 C/m^2 on the OMM and 0.001 C/m^2 on the IMM surface. The excitation field is 1.0 V/cm.

the fact that the field inside a single membrane is spatially uniform. This approximation should be better for larger membrane separations and is expected to give less accurate results on the IMM because of the 0.05 μm separation between the IMM and the OMM. We performed finite element numerical calculations using QuikField (33) to test the field uniformity between the IMM and the OMM. The field is completely uniform, modeling only permittivity variations inside the mitochondria. Fig. 9 shows the two-membrane finite element calculation of (*a*) the potential distribution and (*b*) the electric field distribution at 1 MHz. The finite element mesh is also shown in *b*. This calculation was performed with dimensions and parameters given in Table 1 without mobile surface charges and for an electric field excitation of 1.0 V/cm. Regions from left to right in *a* and *b* include the matrix, IMM, inner membrane space, OMM, and suspending medium. These calculations do not show appreciable field distortions in the region between the IMM and the OMM. Greater field uniformity is observed for higher matrix and IMM conductivity values. From the finite element analysis, we conclude that the spherical approximation to the convoluted IMM is probably a greater limiting factor than the shells' proximity.

We find that mobile surface charges increase the induced membrane potentials but do not significantly affect the frequency where the induced potentials are maximal. Most of the potential drop occurs across the plasma membrane at low frequencies. For mitochondrial membranes in whole cells, there will be no effect of applied ac fields at lower frequencies, as the field cannot penetrate the plasma membrane. Transmembrane potentials are induced across the mitochondrial outer and inner membranes at higher excitation frequencies in whole cells according to the three-membrane model.

The two-membrane model shows that isolated mitochondria exhibit a frequency response in external fields different from the mitochondria in cells. This is because the electric field is not screened by the plasma membrane at low frequencies as it is in whole cells. The induced potential across IMM can cause conformational changes in the embedded membrane proteins. These conformational changes can affect metabolic processes in the mitochondria and give rise to harmonic generation at multiples of the excitation frequency. We find that the induced IMM potential is highly sensitive to changes in matrix conductivity, both increasing and shifting dramatically to lower frequencies with decreasing matrix conductivity. According to the chemiosmotic model, energy stored in the transmembrane electrochemical gradient is converted into the bond energy of ATP by the ATP synthase. The proton motive force (PMF) (34)

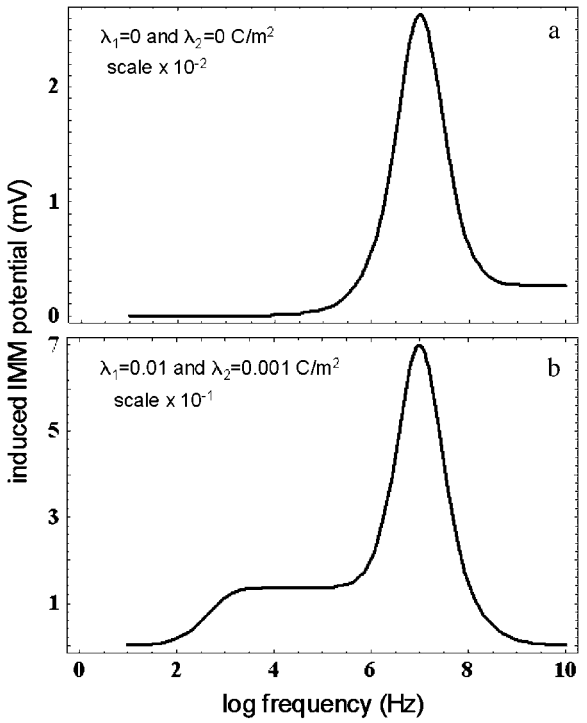

FIGURE 7 Variation of the induced potential across the IMM with frequency of the excitation field in the isolated mitochondrion, two-membrane model (*a*) without free charges and (*b*) with a surface charge density of 0.01 C/m^2 on the OMM and 0.001 C/m^2 on the IMM surface. The excitation field is 1.0 V/cm.

$$PMF = \frac{2.3RT}{F}\Delta pH + \Delta\Phi \tag{33}$$

drives the production of ATP, where R is the universal gas constant and F is the Faraday constant. The proton gradient ΔpH contributes ~60 mV with $\Delta\Phi$~140 mV for a net PMF of ~200 mV. This corresponds to a change in free energy $\Delta G = -4.6$ kcal/mole for each proton translocation. Our calculations show that the inner mitochondrial membrane $\Delta\Phi$ is modulated by 0.66 mV ($\Delta G = -15.2$ cal/mole) in whole cells and by ~0.75 mV ($\Delta G = -17.3$ cal/mole) in isolated mitochondria (for a matrix conductivity of 0.1 S/m) for each V/cm increment in an excitation field at 10^5 Hz. For example, a 10 V/cm amplitude excitation field modulates the intrinsic mitochondrial (IM) by ±7.5 mV. This oscillatory component, when added to the existing membrane potential, could easily modulate the conformational states of the IM complexes, resulting in nonlinear harmonic response. At higher matrix conductivity values, $\Delta\Phi$ decreases and peaks at higher frequencies. We also find that the induced transmembrane potentials increase with both lower membrane permittivity and conductivity by an amount depending on the excitation frequency.

The theoretical results reported here are qualitatively consistent with experimental studies (8) suggesting that ac electric fields can be used to noninvasively probe internal

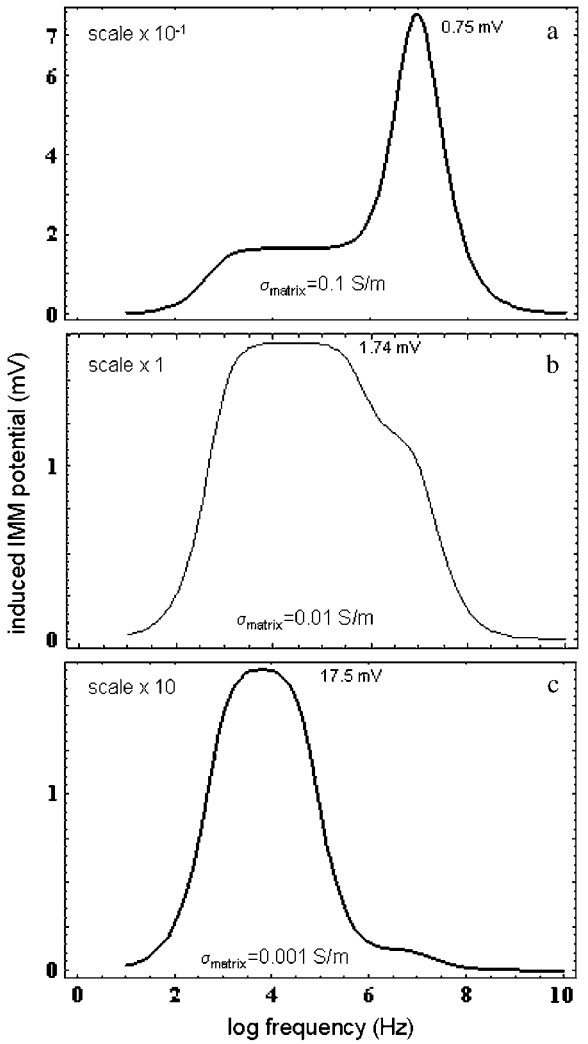

FIGURE 8 Change in induced inner mitochondrial transmembrane potential with frequency of the excitation field for matrix conductivities of (*a*) 0.1, (*b*) 0.01, and (*c*) 0.001 S/m. The excitation field is 1.0 V/cm.

membranes, such as the mitochondrial membranes, within a live cell. It has been shown that membrane macromolecules can directly respond to fields of the order 10^{-2} –10^{-3} V/cm depending on cell geometry (35,36). It is considerably more complicated to quantitatively study mitochondrial transmembrane potentials using ratiometric fluorescent imaging (37) than patch-clamp measurements of plasma membrane potentials. Patch-clamp measurements are clearly not possible for mitochondria or for measuring properties involving the collective average behavior of large numbers of cells—such as ac conductivity and dielectric permittivity—that do not depend on changes in membrane protein conformational states. It has been shown that the linear dielectric response of cells in suspension directly correlates with the membrane potential (24). It may thus be possible to calculate a specific organelle's contribution to the dielectric permittivity. These results are therefore potentially significant, both for fundamental studies

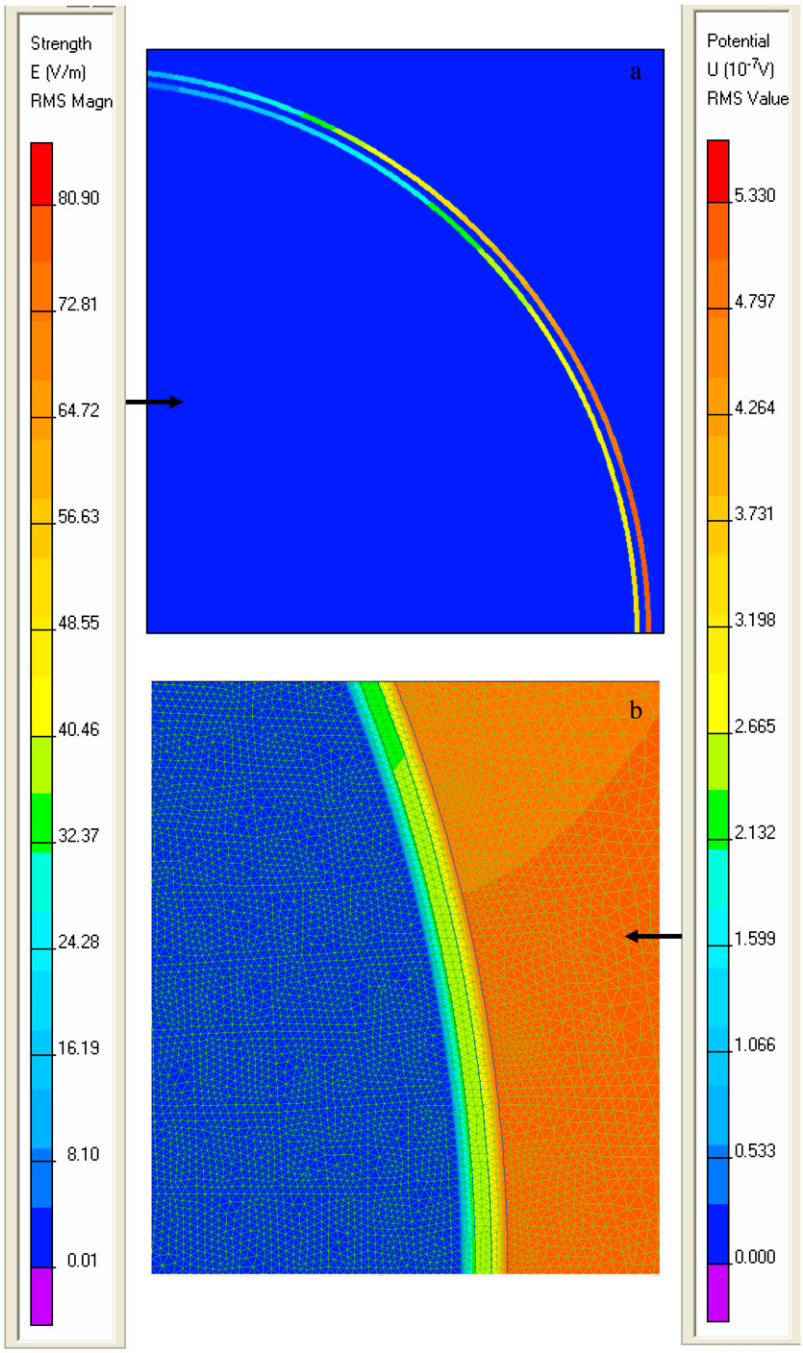

FIGURE 9 Finite element calculation showing the distribution of (*a*) potential and (*b*) electric field strength in the two-membrane model at 1 MHz with parameters and dimensions given in Table 1. The partial cross section near the polar cap of the mitochondrion shows the matrix, IMM, inner membrane space, OMM, and suspending medium. The excitation field is 1.0 V/cm incident from right to left in this figure.

in biology and biophysics and for biomedical applications. However, further work is needed to properly take into account the complex geometries of the mitochondrial inner membrane and other internal membranes.

The authors gratefully acknowledge the referee's helpful comments and suggestions regarding, among other things, nonlinear charge and conductivity relations. We are also grateful for helpful conversations with Dharmakeerthi Nawarathna and Gustavo Cardenas.

J.H.M. and V.V. thank the Robert A. Welch Foundation (E-1221) and state of Texas through the Texas Center for Superconductivity at the University of Houston for financial support. J.H.M. also gratefully acknowledges support by grant No. R21CA122153 from the National Heart, Lung, and Blood Institute and the National Cancer Institute, National Institutes of Health, and from the National Science Foundation. The content is solely the responsibility of the authors and does not necessarily represent the official views of the above agencies.

REFERENCES

1. Heller, R., R. Gilbert, and M. J. Jaroszeski. 1999. Clinical applications of electrochemotherapy. *Adv. Drug Deliv. Rev.* 35:119–129.
2. Golzio, M., M. P. Rols, and J. Teissié. 2004. In vitro and in vivo electric field-mediated permeabilization, gene transfer, and expression. *Methods.* 33:126–135.

3. Astumian, R. D. 1993. Effects of time-dependent electric fields on membrane transport. *Biophys. J.* 64:7–8.

4. Astumian, R. D., and I. Derényi. 1998. Fluctuation driven transport and models of molecular motors and pumps. *Eur. Biophys. J.* 27:474–489.

5. Woodward, A. M., and D. B. Kell. 1990. On the nonlinear dielectric properties of biological systems. Saccharomyces cerevisiae. *Bioelectrochem. Bioenerg.* 24:83–100.

6. Woodward, A. M., and D. B. Kell. 1991. On the relationship between the nonlinear dielectric properties and respiratory activity of the obligately aerobic bacterium Micrococcus luteus. *Bioelectrochem. Bioenerg.* 26:423–439.

7. Tsong, T. Y. 1988. Active cation pumping of Na^+, K^+ATPase and sarcoplasmic reticulum Ca^{2+}ATPase induced by an electric field. *Methods Enzymol.* 157:240–251.

8. Miller, J. H. Jr., D. Nawarathna, V. Vajrala, J. Gardner, and W. R. Widger. 2005. Electromagnetic probes of molecular motors in the electron transport chains of mitochondria and chloroplasts. *J. Phys. IV Colloq.* 131:363–366.

9. Nawarathna, D., J. H. Miller Jr., J. R. Claycomb, G. Cardenas and D. Warmflash. 2005. Harmonic response of cellular membrane pumps to low frequency electric fields. *Phys. Rev. Lett.* 95:158103.

10. Nawarathna, D., J. R. Claycomb, G. Cardenas, J. Gardner, D. Warmflash, J. H. Miller Jr. and W. R. Widger. 2006. Harmonic generation by yeast cells in response to low-frequency electric fields. *Phys Rev E.* 73:051914.

11. Lowell, B. B., and G. I. Shulman. 2005. Mitochondrial dysfunction and type 2 diabetes. *Science.* 307:384–387.

12. Huss, J. M., and D. P. Kelly. 2005. Mitochondrial energy metabolism in heart failure: a question of balance. *J. Clin. Invest.* 115:547–555.

13. Warburg, O. 1930. The Metabolism of Tumors. Arnold Constable, London.

14. Petersen, P. L. 1978. Tumor mitochondria and the bioenergetics of cancer cells. *Prog. Exp. Tumor Res.* 22:190–274.

15. Swerdlow, R. H., and S. J. Kish. 2002. Mitochondria in Alzheimer's disease. *Int. Rev. Neurobiol.* 53:341–385.

16. Schwan, H. P. 1957. Electrical properties of tissue and cell suspensions. *Adv. Biol. Med. Phys.* 5:147–209.

17. Grosse, C., and H. P. Schwan. 1992. Cellular membrane potentials induced by alternating fields. *Biophys. J.* 63:1632–1642.

18. Kotnik, T., F. Bobanović, and D. Miklavčič. 1997. Sensitivity of transmembrane voltage induced by applied electric fields—a theoretical analysis. *Bioelectrochem. Bioenerg.* 43:285–291.

19. Fricke, H. 1953. The electric permittivity of a dilute suspension of membrane-covered ellipsoids. *J. Appl. Phys.* 24:644–646.

20. Bryant, G., and J. Wolfe. 1987. Electromechanical stresses produced in the plasma membranes of suspended cells by applied electric fields. *J. Membr. Biol.* 96:129–139.

21. Jerry, R. A., A. S. Popel, and W. E. Brownell. 1996. Potential distribution for a spheroidal cell having a conductive membrane in an electric field. *IEEE Trans. Biomed. Eng.* 43:970–972.

22. Gimsa, J., and D. Wachner. 1999. A polarization model overcoming the geometric restrictions of the Laplace solution for spheroidal cells: obtaining new equations for field-induced forces and transmembrane potential. *Biophys. J.* 77:1316–1326.

23. Gimsa, J., and D. Wachner. 2001. Analytical description of transmembrane voltage induced on arbitrarily oriented ellipsoidal and cylindrical cells. *Biophys. J.* 81:1888–1896.

24. Prodan, C., and E. Prodan. 1999. The dielectric behavior of living cell suspensions. *J. Phys. D Appl. Phys.* 32:335–343.

25. Asami, K., and A. Irimajiri. 1984. Dielectric analysis of mitochondria isolated from rat liver II. Intact mitochondria as simulated by a double-shell model. *Biochim. Biophys. Acta.* 778:570–578.

26. Kotnik, T., and D. Miklavčič. 2000. Analytical description of transmembrane voltage induced by electric fields on spheroidal cells. *Biophys. J.* 79:670–679.

27. Kotnik, T., and D. Miklavčič. 2006. Theoretical evaluation of voltage inducement on internal membranes of biological cells exposed to electric fields. *Biophys. J.* 90:480–491.

28. Woodward, A. M., and D. B. Kell. 1991. Dual-frequency excitation: a novel method for probing the nonlinear dielectric properties of biological systems, and its application to suspensions of S. cerevisiae. *Bioelectrochem. Bioenerg.* 25:395–413.

29. Nawarathna, D., J. R. Claycomb, J. H. Miller Jr., and M. J. Benedik. 2004. Nonlinear dielectric spectroscopy of live cells using superconducting quantum interference devices. *Appl. Phys. Lett.* 86:023902.

30. Schoenbach, K. H., R. P. Joshi, J. F. Kolb, N. Chen, M. Stacey, P. F. Blackmore, E. S. Buescher, and S. J. Beebe. 2004. Ultrashort electrical pulses open a new gateway into biological cells. *Proc. IEEE.* 92:1122–1137.

31. Yang, Y. H., Y. L. Qiu, C. T. Xie, H. Q. Tian, Z. Zhang, and S. D. Russell. 2005. Isolation of two populations of sperm cells and microelectrophoresis of pairs of sperm cells from pollen tubes of tobacco (*Nicotiana tabacum*). *Sex Plant Reprod.* 18:47–53.

32. Nelson, P. 2003. Biological Physics: Energy, Information, Life. W. H. Freeman, New York. 142.

33. QuickField by Tara Analysis Ltd. QuickField: A New Approach to Field Modeling. http://www.quickfield.com.

34. Oster, G., H. Wang, and M. Grabe. 2000. How F_0-ATPase generates rotary torque. *Philos. Trans. R. Soc. Lond. B Biol. Sci.* 355:523–528.

35. Weaver, J. C., T. E. Vaughan, R. K. Adair, and R. Dean Astumian. 1998. Theoretical limits on the threshold for the response of long cells to weak extremely low frequency electric fields due to ionic and molecular flux rectification. *Biophys. J.* 75:2251–2254.

36. Weaver, J. C., and R. Dean Astumian. 1990. The response of living cells to very weak electric fields: the thermal noise limit. *Science.* 247:459–462.

37. Duchen, M. R., J. Jacobson, J. Keelan, M. H. Mojet, and O. Vergun. 2001. Functional Imaging of Mitochondria within Cells. *In* Methods in Cellular Imaging. A. Periasamy, editor. American Physiological Society, Oxford/New York. 88–111.